Nuclear Engineering and Technology 57 (2025) 103295

Contents lists available at ScienceDirect

Nuclear Engineering and Technology

journal homepage: www.elsevier.com/locate/net

Original Article

Gamma radiation attenuation, mechanical properties and microstructure of barite-modified cement and geopolymer mortars

Daria Jóźwiak-Niedźwiedzka [a,*], Pavel Rovnaník [b], Mariusz Dąbrowski [a], Jakub Ośko [c], Michał Kuć [c], Maciej Maciak [c]

[a] Institute of Fundamental Technological Research, Polish Academy of Sciences, Pawińskiego 5B, 02-106, Warsaw, Poland
[b] Faculty of Civil Engineering, Brno University of Technology, Veveří 331/95, 612 00, Brno, Czech Republic
[c] National Centre for Nuclear Research, ul. A. Sołtana 7, 05-400, Otwock, Poland

ARTICLE INFO

Keywords:
Cement mortar
Fly ash geopolymer mortar
Barite
Gamma ray attenuation
Microstructure

ABSTRACT

The present study contributes to the development of alternative materials for radiation shielding, focusing on environmental sustainability and material cost efficiency. The primary aim was to evaluate the compressive and flexural strength, mineral composition, microstructure, and gamma-ray attenuation properties of cement mortars and geopolymer mortars containing barite powder. Mortars based on ordinary Portland cement (OPC) and fly ash geopolymers with varying amounts of barite powder were assessed for their shielding properties at energy levels associated with the decay of ^{137}Cs. From the results, key parameters such as the linear attenuation coefficient (μ), mass attenuation coefficient (μ_m), half-value layer (HVL), and tenth-value layer (TVL) were determined. The results showed that while cement-based composites exhibited superior gamma radiation attenuation compared to fly ash geopolymer mortars, the latter had higher mass attenuation efficiency, meaning less material density was required for the same level of shielding. Additionally, cement mortars had 23–25 % higher mechanical strength than geopolymer mortars. Importantly, the inclusion of barite powder improved the radiation shielding performance of both materials by 7–10 %, demonstrating its effectiveness in enhancing the protective properties of these mortars. This research highlights the potential of fly ash geopolymer mortars as viable, eco-friendly alternatives to traditional cement mortars in radiation shielding applications.

1. Introduction

Nuclear materials – including those used in nuclear reactors, radioactive waste, and medical imaging – pose unique challenges due to their ionizing radiation, [1–4]. Effective management and containment are crucial for safety and minimizing environmental and health risks. A key aspect of managing nuclear materials involves effective radiation shielding to protect humans and the environment from gamma radiation, [5,6].

Gamma rays are high-energy electromagnetic waves with significant penetrating power, making them difficult to shield against. They are commonly emmited by radioactive isotopes in nuclear power plants and used in medical imaging. As a result, materials used for shielding in these contexts must be carefully selected for their gamma-ray attenuation capabilities [7,8].

Cement based composites have traditionally been employed for radiation shielding due to their density, strength, durability and versatility [9,10]. However, their structural integrity and long-term performance can be affected by exposure to gamma radiation [11]. This interaction, particullary in concrete structures exposed to gamma radiation in industrial and research settings, impacts both mechanical and chemical properties [12–15]. Understanding how gamma radiation affects concrete at the atomic and molecular levels is essential for applications such as nuclear power plants, radioactive waste storage, and certain medical facilities. In tandem with increasing environmental concerns, there is growing interest in alternative materials that offer similar or better performance with reduced envinromental impact. In 2013, the International Atomic Energy Agency (IAEA) expressed interest in four alternative cementitious materials: geopolymers, magnesium phosphate cements, calcium aluminate cements, and calcium sulfoaluminate cements [3,4]. Despite progress, further work is needed on process optimization, precursor standardization, and durability

* Corresponding author.
E-mail addresses: djozwiak@ippt.pan.pl (D. Jóźwiak-Niedźwiedzka), rovnanik.p@vutbr.cz (P. Rovnaník), mdabrow@ippt.pan.pl (M. Dąbrowski), Jakub.Osko@ncbj.gov.pl (J. Ośko), Michal.Kuc@ncbj.gov.pl (M. Kuć), Maciej.Maciak@ncbj.gov.pl (M. Maciak).

https://doi.org/10.1016/j.net.2024.10.057
Received 6 August 2024; Received in revised form 2 October 2024; Accepted 29 October 2024
Available online 30 October 2024

assessments before widespread adoption of these alternative materials.

Geopolymers are a promising alternative to materials like glass [16,17], modified plastics [18] or red mud [19,20] which currently undergoing intensive study. These inorganic materials are produced via low-temperature polycondensation of aluminosilicate precursors in an highly alkaline solution. They are classified as alkali-activated materials where the binding phase consists of aluminosilicate, forming an amorphous to semicrystalline 3D network of interconnected SiO_4 and AlO_4 tetrahedra. This network, resembling a pseudo-zeolite structure, differs from the chain-like calcium silicate hydrates in traditional cements. The aluminosilicate precursors can include calcined materials such as metakaolin, or various waste materials like fly ash from the combustion of coal, rise husk ash, straw ash, bottom ash [21–25], red mud [26,27], or waste red brick powder [28,29]. Using waste materials provides both economic and environmental benefits, making fly ash-based geopolymer an attractive alternative. Alkali activation of fly ash has been extensively studied [30–36], offering economic advantages and providing higher durability and resistance to aggressive acids [37,38], alkali-aggregate reaction [39,40], and high temperature exposure [41–43].

Few studies have examined the effect of high-energy radiation alkali-activated materials or geopolymers. Those that have compared shielding properties between alkali-activated slag and Portland cement found higher shielding capacities and better gamma irradiation resistance in slag-based materials [44–46]. Studies on fly ash-based glasses with barium–borate have reported superior gamma-ray shielding compared to standard concrete [47], while composites with barium sulfate have demonstrated potential to replace lead shielding in X-ray applications [48]. Further research has revealed that low doses of gamma radiation can enhance geopolymerization, though high doses may lead to structural degradation [49–51]. Fly ash-based geopolymers have shown comparable HVL and TVL to Portland cement concrete at low energy levels but were less effective at higher energies [52]. Metakaolin and fly ash geopolymer composites have been reported to exhibit a lower linear attenuation coefficient for gamma irradiation compared to cement composites, but they are more efficient at attenuating thermal neutrons [53]. Ahn et al. demonstrated that metakaolin-based geopolymers can be used to solidify sulfate-rich nuclear waste [54]. Research by Catenacci et al. [55] showed that although fly ash samples from different sources varied in chemical composition, these differences among Class C fly ashes resulted in only marginal changes in the linear attenuation coefficient. Instead, changes in aggregate quantity and composition had a more pronounced impact. Furthermore, gamma rays had negligible effects on the pore structure of the geopolymer, indicating that irradiation does not lead to significant structural changes. However, the dose rate does influence the radiolysis of water and the hydrogen production [56].

This study compares the shielding performance of cement-based and fly ash geopolymer mortars containing barite powder as a partial replacement of quartz sand. Barite, a high-density mineral, increases the mortar's density, which is beneficial for radiation shielding applications. Additionally, barite particles serve as fillers, enhancing the mechanical properties of the mortar. The prepared mixtures were comprehensively tested and analyzed for their microstructure and mechanical properties. The main objective was to evaluate the ability of these materials to attenuate low-energy gamma radiation from ^{137}Cs gamma-ray source (662 keV). Fly ash geopolymer is a more sustainable, environmentally friendly, and cost-effective material compared to ordinary Portland cement, making it a potential alternative shielding material in non-load-bearing applications where high mechanical strength is not essential. The research provides new and original insights into the comparison of cement mortars and fly ash geopolymer mortars containing barite powder, with a focus on their mechanical properties, microstructure, and gamma-ray attenuation capabilities.

2. Materials and methods

2.1. Materials

2.1.1. Geopolymer based composites

Geopolymer mortars were prepared using fly ash from the high-temperature combustion of coal at the Dětmarovice Power Plant (CZ). A comercial water glass solution (Vodní sklo, CZ) combined with a 40 % sodium hydroxide solution served as the alkaline activator. The fine aggregate used was standard natural siliceous sand, conforming to EN 196–1 [57], with a specific gravity of 2.65 g/cm^3 and a maximum grain size of 2 mm. Tap water was also used in the mixture. Barite powder (<0.5 mm, specific gravity 4.20 g/cm^3 was used as a partial replacement for the sand by mass. The specimens were labeled as follows: the reference mix without barite powder was denoted GEO, while those with 10 % and 20 % barite powder were labeled GEO-B-10 and GEO-B-20, respectively. The chemical compositions of the fly ash and water glass are presented in Table 1, while Table 2 shows the chemical composition of barite powder. The compositions of the tested geopolymer mortars are summarized in Table 3. The water-to-fly ash ratio was 0.53, including water from both the alkaline activator mixture and additional mixing water. Four prisms (40 × 40 × 160 mm) were cast for each composition. Three prisms were used to determine the mechanical properties and for microstructural analysis, while one prism was reserved for gamma radiation tests. After casting, the molds were sealed with PE foil to prevent water evaporation and cured for 24 h in an electric furnace at 60 °C to accelerate the setting. Following this, the specimens were placed in a plastic bags and stored under laboratory conditions (22 ± 2 °C) according to standard procedure until testing.

2.1.2. Cement based composites

In all the cement mortar mixes, ordinary Portland cement (CEM I 42.5R) was used along with a fine aggregate - standard natural siliceous sand in accordance with EN 196–1 [57]. The sand had a specific gravity of 2.65 g/cm^3 and a maximum grain size of 2 mm. Tap water was utilized for mixing. Barite powder served as a substitute for sand, and the same amount of barite was incorporated in both the geopolymer and cement mortar. The specimens were labeled as follows: reference without barite powder (CEM), and those containing 10 % and 20 % barite powder as CEM-B-10, and CEM-B-20, respectively. The chemical composition of cement is provided in Table 4, while Table 5 outlines the composition of cement mortars. A constant water to binder ratio of 0.5 was maintained for all mixes. Four prisms (40 × 40 × 160 mm) were cast for each composition for mechanical and microstructural analysis. All specimens were cured in water at the temperature of 20 ± 1 °C for 28 days, following the standard procedure before testing.

2.2. Methods

2.2.1. Mineral and chemical composition

The mineral composition of fly ash geopolymers and cement mortars was analyzed using X-ray diffraction (XRD). After 28 days of curing, the mortar specimens were dried at 50 °C for three days, crushed into small pieces (1 mm diameter), and ground using a ceramic mortar. The ground material was sieved through a 0.032 mm sieve. A Bruker D8 DISCOVER diffractometer with a 40 kV voltage and 40 mA lamp current, equipped with a copper lamp as an X-ray source, was used. Diffraction patterns were collected over a 2θ range from 5° to 65° with a step size of 0.02° and a 1-s counting time using coupled theta-2theta geometry. The Diffrac.Eva V5.2 software was utilized to analyze the XRD patterns and determine the crystallite phases.

Fourier-Transform Infrared Spectroscopy (FTIR) was employed to analyze the chemical composition of the specimens, prepared similarly to those for XRD analysis. FTIR measurements were conducted with a the Bruker Vertex 70 equipment in ATR mode (Bruker Platinum Diamond ATR stage), with 8 scans averaged at a 2 cm^{-1} resolution.

Table 1
Chemical composition and LOI of fly ash and water glass in wt.% by XRF.

	SiO_2	Al_2O_3	Fe_2O_3	MgO	CaO	SO_3	Na_2O	K_2O	TiO_2	MnO	P_2O_5	LOI
Fly ash	51.67	23.31	7.08	0.36	4.45	0.01	0.77	2.95	1.00	1.14	0.04	5.83
WG[a]	29.53	–	–	–	–	–	16.96	–	–	–	–	–

[a] Content of H_2O in WG was equal to 53.51 %.

Table 2
Chemical composition of barite rock and LOI in wt.% by XRF.

SiO_2	Al_2O_3	Fe_2O_3	MgO	CaO	SO_3	Na_2O	BaO	TiO_2	Mn_2O_3	SrO	LOI
4.88	0.15	0.26	0.14	2.39	30.23	0.04	59.26	0.10	0.06	1.43	1.10

Table 3
The mixture proportions of geopolymer mortars.

Mix ID	Fly ash (g)	WG (g)	40 % NaOH	Quartz sand (g)	Baryte (g)	Water (ml)
GEO	350	253	27	1050	–	30
GEO-B-10	350	253	27	940	175	30
GEO-B-20	350	253	27	830	350	30

Background scans were performed before sample scan to account for humidity and carbon dioxide fluctuations in the air. All scans were conducted under ambient conditions (~25 °C, 50 % relative humidity).

2.2.2. Density and mechanical properties

After 28 days of curing, density was determined by measuring the dimensions and weight of the specimens. Flexural and compressive strength tests followed the procedures outlined in EN 196–1 [57], three-point loading with standardized 40 × 40 × 160 mm beams. The EZ testing machine (50 kN load capacity, loading rate of 50 N/s) was used to determine flexural strength, while a 2000 kN Controls testing machine, applying a constant loading rate of 500 N/s, was employed to determine compressive strength. Each test was completed when the specimens failed and split into two parts, resulting in three flexural strength values and four compressive strength values per mortar type. The remaining halves of the mortar beams were retained for further testing.

2.2.3. Microstructure

The microstructure of both fly ash geopolymer and cement mortar specimens was examined using a JEOL JSM-6460 LV high-vacuum scanning electron microscope (SEM). Fresh split surfaces were anayzed using secondary electrons (SE), while polised surfaces were studied with back-scattered electrons (BSE). Specimens were carbon-coated, and conductive tape was applied to ensure conductivity. A voltage of 15 kV and an aperture of 120 μm were applied, maintaining a working distance of 9–11 mm. Observations were conducted at magnification ranging from 30 × to 300 × .

Nitrogen adsorption/desorption experiments (BET analysis) were conducted after 28 days of curing to analyze the pore structure. Specimens were prepared as per the XRD procedure, and measurements followed the Barret-Joyner-Halenda (BJH) method using a Quantachrome Autosorb IQ analyzer. The samples were degassed at 105 °C for 2 h to remove moisture and gas contaminants, in accordance with the standard for this characterization. Compared to the long-term vacuum drying process at low temperature, the short-term degassing process is more suitable for the pretreatment of the samples to be analyzed in this technique [58,59]. The desorption isotherms as well as the pore size distribution and the cumulative volume of pores registered from 1 nm to 100 nm were obtained as test results.

2.2.4. Gamma-ray attenuation parameters

To estimate the gamma-ray attenuation parameters, a test stand was prepared according to the EN 61331-1 standard [60,61] (Fig. 1). The tests were conducted in an accredited calibration laboratory (accreditation No. AP 070 issued by the Polish Center for Accreditation). Based on the previous investigation on radiation shielding of concrete slabs [61], measurements were performed using a Tema Sinergie IM6M automatic irradiator with ^{137}Cs gamma-ray reference source and a G5 type graphite ionization chamber [62]. The active center of the detector was set at a distance of 85 cm from the source, at a point with an air kerma rate of $\dot{K}_{air} = 30.4 \pm 1.5$ mGy h^{-1}.

Based on dosimetric measurements, the linear attenuation coefficient (μ), the half-value layer (HVL), and the tenth-value layer (TVL) were determined. The linear attenuation coefficient was obtained as a

Table 5
The mixture proportions of cement mortars.

Mix ID	Cement [g]	Water [ml]	Quartz sand [g]	Barite [g]
CEM	450	225	1350	–
CEM-B-10	450	225	1245	175
CEM-B-20	450	225	1140	350

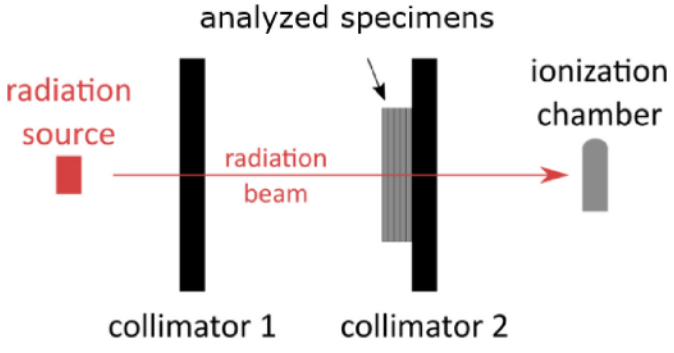

Fig. 1. Schematic view of the gamma-ray attenuation test stand.

Table 4
Chemical composition and LOI of cement CEM I 42.5R in wt.% by XRF.

SiO_2	Al_2O_3	Fe_2O_3	MgO	CaO	SO_3	Na_2O	K_2O	TiO_2	MnO	P_2O_5	LOI
19.26	4.72	3.21	2.88	61.86	3.12	0.22	0.93	0.24	0.09	0.13	3.10

curve-fitting parameter of the attenuation rate (k) dependent on the thickness of the shielding layer (d). The attenuation rate (k) is defined as the ratio of the ionization current of the ionization chamber without a shield i_0 to the value of the ionization current behind a shield of thickness d, $i(d)$:

$$k(d) = \frac{i_0}{i(d)} \tag{1}$$

$$k(d) = e^{\mu d} \tag{2}$$

The HVL and TVL were calculated from μ:

$$HVL = \frac{\ln(2)}{\mu} \tag{3}$$

$$TVL = \frac{\ln(10)}{\mu} \tag{4}$$

The mass attenuation coefficient, which characterizes how easily a material can be penetrated by gamma radiation, was calculated as the attenuation coefficient normalized to density:

$$\mu_m = \frac{\mu}{\rho} \tag{5}$$

The study of radiation attenuation by concrete specimens was carried out for five shielding layer thicnesses. The relative uncertainty in determining the attenuation rate k for all settings did not exceed 5 %. The uncertainty μ (u_μ) was determined as the uncertainty of curve fitting by the least squares method. The uncertainties of HVL and TVL were determined from the uncertainty of u_μ as follows:

$$u_{HVL} = HVL \bullet \frac{u_\mu}{\mu} \tag{6}$$

$$u_{TVL} = TVL \bullet \frac{u_\mu}{\mu} \tag{7}$$

After 28 days, previously cast specimens of 40 × 40 × 160 mm were cross-cut into 9 mm thick slices. Five consecutive slices were placed between collimators 1 and 2 (Fig. 1) and irradaited.

3. Results and discussion

3.1. Mineral and chemical composition

The X-ray diffraction (XRD) mineral analysis, shown in Figs. 2 and 3, indicates the presence of crystalline phases in the analyzed specimens, derived from the used starting materials used. In geopolymer specimens, quartz, mullite, and hematite were identified, while in cement mortars, quartz and portlandite were detected. As seen in Fig. 2, quartz and mullite were the major crystalline phases, while hematite was a minor in the reference geopolymer specimen. These phases originated from the fly ash, which contained crystalline material without pozzolanic reactivity [63]. However, much of the matter in both geopolymer and cement binder is amorphous and not observable via XRD. New characteristic peaks were observed in the XRD patterns of modified mortars, corresponding to the partial replacement of quartz sand with barite powder, consistent with previously published data [64,65]. The intensity of these peaks increased with barite content, Figs. 2 and 3.

The chemical composition of the specimens, determined by Fourier-Transform Infrared Spectroscopy (FTIR), is shown in Figs. 4 and 5. To facilitate comparisons, data for both barite and the analyzed mortars were included. Upon analyzing the FTIR spectral profile of the reference cement mortar (CEM), the following features were identified:

- A strong band at 452 cm^{-1} with a shoulder at 513 cm^{-1}, associated with in-plane and out-of-plane Si-O vibrations.
- A broadband in the 800–1250 cm^{-1} range, centered at 1035 cm^{-1} with a shoulder at 1163 cm^{-1}, attributed to the stretching mode of Si-O bond SiO_4 tetrahedra.
- Bands at 796, 777, and 694 cm^{-1} attributed to the symmetrical stretching and bending Si-O vibrations{Saikia, 2014 #117}.
- Bands at 1472, 1419, and 876 cm^{-1} corresponding to carbonate species.
- Broadband in the 3100–3600 cm^{-1} range, along with a weak band at 1647 cm^{-1}, attributed to the OH stretching and bending modes in water associated with the cement matrix [66].
- The presence of a peak related to the OH stretching vibrations of portlandite at 3643 cm^{-1} [66].

In the FTIR spectra of the reference geopolymer mortar, the following features were identified:

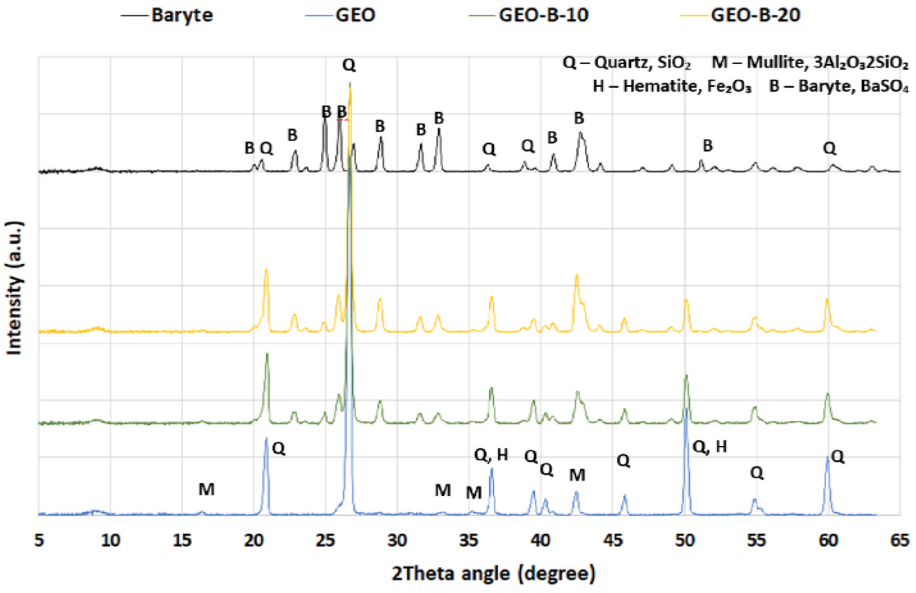

Fig. 2. XRD diffractogram for the fly ash geopolymer mortars.

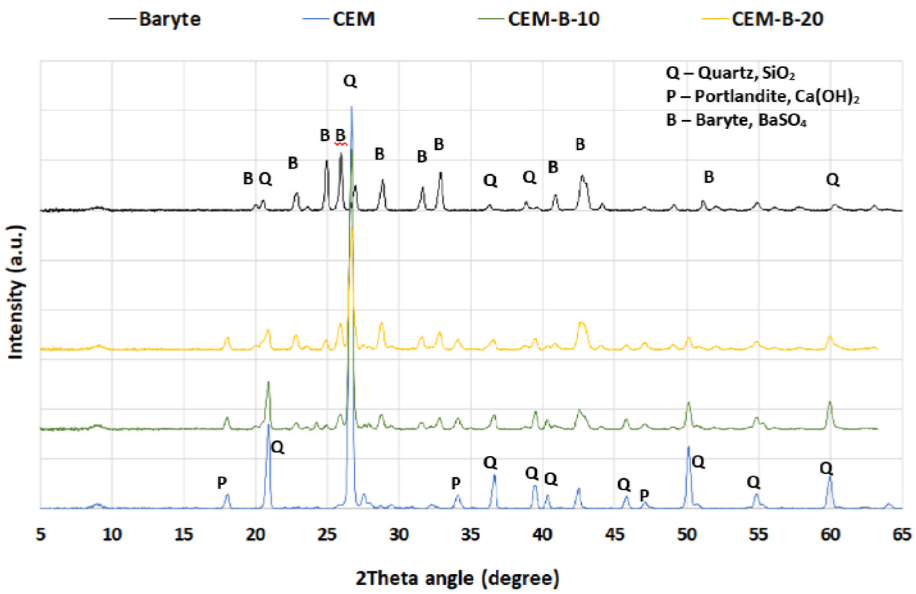

Fig. 3. XRD diffractogram for the cement mortars.

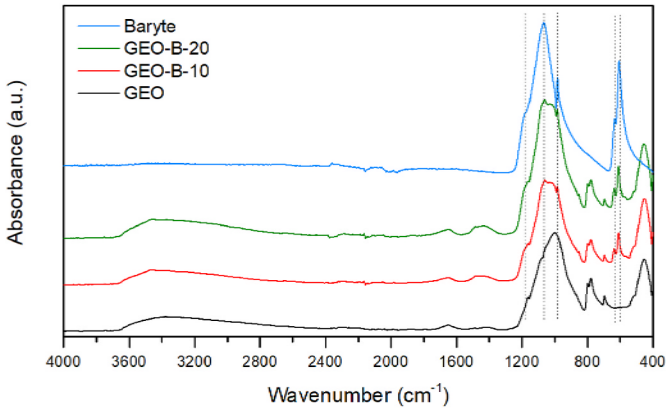

Fig. 4. FTIR spectra for the fly ash geopolymer based mortars.

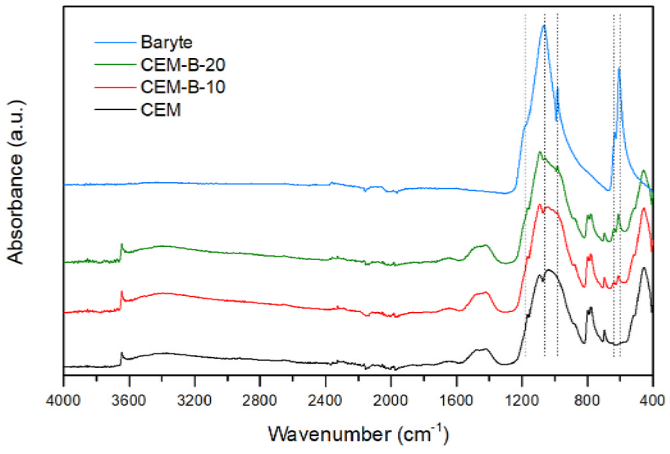

Fig. 5. FTIR spectra for the cement based mortars.

- A band at 452 cm^{-1} with a shoulder at 513 cm^{-1}, associated with in-plane and out-of-plane Si-O vibrations.
- Bands at 796, 777, and 694 cm^{-1} assigned to the symmetrical stretching and bending Si-O vibrations.
- Broadband in the 800–1250 cm^{-1} range, centered at 1000 cm^{-1} with shoulders at 1163 and 1080 cm^{-1}, attributed to the asymmetrical stretching mode of Si-O and Al-O bonds.
- Broad band at 1412 cm^{-1} that corresponds to the carbonates.
- Weak broad bands centered at 3360 and 1648 cm^{-1} attributed to the OH stretching and bending modes, respectively, in water associated with the geopolymer matrix.

The bands at 1163, 1090, 796, 777, 694, 513, and 452 cm^{-1} are associated with quartz, present as aggregate in both types of mortars [67,68]. The presence of barite in the mortars (CEM-B-10, CEM-B-20, GEO-B-10, and GEO-B-20) is confirmed by bands at 1058, 982, 635, and 608 cm^{-1}. The former two bands are linked to asymmetrical and symmetrical stretching vibrations of SO_4^{2-} [69], while the latter two are attributed to the out-of-plane bending vibration of SO_4^{2-} group [69]. In fly ash geopolymer, the broad peak centered around 1000 cm^{-1} can be assigned to Si-O-T (T = Si or Al) asymmetric stretching vibrations in the geopolymer's 3D aluminosilicate structure [70–72] The shift of the peak from 1000 cm^{-1} to approximately 1061 cm^{-1} is attributed to the addition of barite. In the case of cement-based mortars, the strong band at 1035 cm^{-1} with a shoulder at 1046 cm^{-1}, is associated with asymmetric stretching vibrations in C-S-H gels. However, the slight shif towards a higher wavenumber compared to literature data [66,73,74] may result from a higher condensation degree of SiO_4 tetrahedra in the C-S-H phase. It can be concluded that no influence the molecular structure of fly ash geopolymer or cement matrix, as there are no significant differences in the FTIR spectra between reference mortars and mortars containing 10 % and 20 % barite powder, aside from the increased intensity of signals associated with barite.

3.2. *Density and mechanical properties*

The density of the tested specimens is presented in Table 6 and mechanical properties determined after 28 days of curing are presented in Table 7. Geopolymer mortars exhibited lower density compared to cement mortars. The influence of barite powder on mortar density is clearly visible: as the barite content increases, the mortar density also increases, which was expected for both types of mortars [75,76]. The density of the geopolymer mortar with 10 % barite content was approximately equal to the density of the reference cement mortar. However, the density of the geopolymer mortar with 20 % barite content was comparable to the cement mortar with 10 % barite.

Table 6
Density of the fly ash geopolymers and cement mortars, after 28 days of curing.

Specimen description	Density (g cm^{-3})
GEO	2.02 ± 0.03
GEO-B-10	2.16 ± 0.01
GEO-B-20	2.30 ± 0.03
CEM	2.23 ± 0.01
CEM-B-10	2.32 ± 0.01
CEM-B-20	2.44 ± 0.02

Table 7
Mechanical properties of tested fly ash geopolymers and cement mortars.

Specimen description	Compressive strength	Flexural strength
	MPa	
GEO	35.3 ± 0.2	5.9 ± 0.1
GEO-B-10	35.7 ± 0.5	6.5 ± 0.1
GEO-B-20	36.5 ± 0.3	6.4 ± 0.1
CEM	47.3 ± 0.5	7.9 ± 0.2
CEM-B-10	48.0 ± 0.3	8.1 ± 0.1
CEM-B-20	48.5 ± 0.4	8.3 ± 0.1

Geopolymer mortar specimens exhibited approximately 25 % lower compressive and flexural strength compared to cement mortar specimens. The compressive strength of the reference cement mortar was 47.3 MPa, while the reference geopolymer mortar achieved 35.2 MPa. Similary, the flexural strength values were 7.9 MPa and 5.9 MPa, respectively. Replacing part of the fine quartz sand with barite powder resulted in a slight increase in strength, which can be attributed to improved compaction of aggregate particles and densification of the mortar structure. Similar results were reported by Saidani et al. [75], who demonstrated that a minor substitution of sand (5 % by volume) with barite powder (<0.100 mm) did not adversely affect compressive strength. Conversely, Gökçe et al. [77] reported that a higher substitution of fine aggregate with barite (≥50 %) led to a decline in mechanical properties, with a more pronounced negative effect on flexural strength than on compressive strength. However, in this study, no such detrimental effects were observed.

3.3. Microstructure

The microstructure of the reference specimens, including the hardened geopolymer produced through the alkaline activation of fly ash and the hardened cement mortar (both with and without barite powder), was examined using scanning electron microscopy (SEM). Figs. 6 and 7 present SEM images that illustrate the microstructure of the fractured and polished surfaces of the specimens after a 28-day storage duration under air-dry conditions. Evenly distributed angular grains of barite are visible in the micrographs. The SEM image (Fig. 7) reveals incompletely reacted fly ash particles, alongside various products of geopolymerization. The geopolymer matrix results from the reaction between the amorphous components of fly ash and an alkaline activator, with some unreacted fly ash particles still visible. The binding material formed through the alkaline activation of fly ash is observed between the barite particles and sand grains, forming a compact structure bonded to the grain surface (Fig. 7). This material mainly consists of silicon, aluminum, and sodium (Fig. 6). The SEM micrographs also show the presence of microcracks in geopolymer mortar, which likely contribute to the lower flexural strengths by acting as stress concentrators. In

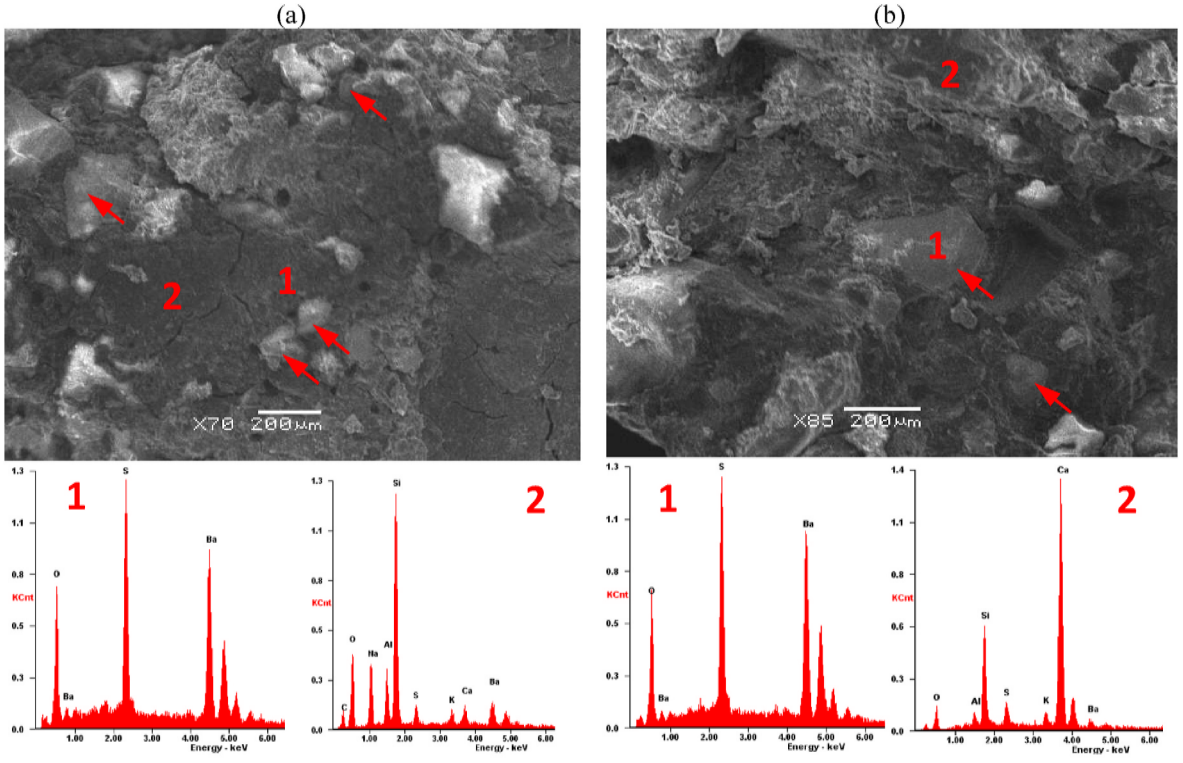

Fly ash geopolymer – GEO-B-10
arrows show barite particles;
(1) Barite particles, (2) geopolymer matrix with traces of barite

Cement mortar – CEM-B-10
arrows show barite particles;
(1) Barite particles, (2) cement matrix with traces of barite

Fig. 6. The microstructure of a: a) geopolymers mortars and b) cement mortars containing barite powder observed on split surfaces using SEM.

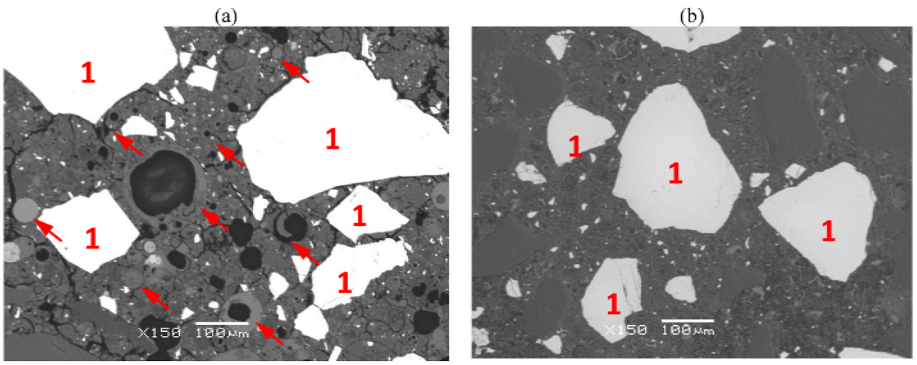

Fig. 7. The microstructure of a: a) geopolymer mortar GEO-B-20, b) cement mortar CEM-B-20 observed on polished surfaces using SEM, 1- barite particles, arrows show fly ash grains.

contrast, the cement specimens exhibit a compact and dense structure, with C-S-H gels filling the spaces between aggregate particles.

SEM analysis further demonstrated the even distribution of barite particles in both the cement and geopolymer matrices. This uniform distribution of barite is significant, as aggregate distribution in concrete affects its gamma-ray attenuation properties [78]. A homogeneous spread of barite particles reduces the paths for gamma radiation, thereby enhancing the material's ability to attenuate and resist the harmful effects of gamma radiation. In the SEM micrographs of geopolymer specimens, circular and smooth fly ash grains are visible, indicating that the alkaline reaction primarily occurs on the surface layer of the fly ash. Similar observations were reported by Rajczyk and Janus [63] on the fracture surfaces of geopolymer specimens with fly ash.

The comprehensive results of the nitrogen adsorption and desorption measurements are provided in Table 8 and visually presented in Figs. 8–10. A monotonic increase in nitrogen adsorption was observed in both reference mortars across relative pressures of 0.1–0.9, followed by a rapid increase at relative pressures between 0.9 and 1.0 (Fig. 8). However, the amount of nitrogen adsorbed by the geopolymer mortar was only half of that observed for the cement mortar. The addition of barite increased nitrogen adsorption in both mortars, although this increase was more pronounced in geopolymer mortars at low relative pressures and in cement mortars at high pressures.

The surface area and pore volume of the reference geopolymer were slightly lower than those of the cement mortar. However, when part of the sand was substituted with barite powder, the surface area, cumulative pore volume, and pore size increased in geopolymer mixes. The greater the barite content, the larger the surface area and the cumulative pore volume. In contrast, the surface area and pore volume of cement-based mortars modified with barite powder remained nearly equal to those of the reference mortar, suggesting that substituting quartz with barite does not significantly affect the microstructure of cement mortar.

Pores smaller than 10 nm are generally classified as gel pores, while those those larger than 10 nm are described as capillary pores [59]. The pore size distribution curves for the geopolymer mortars showed unimodal profiles ranging from 1 to 100 nm, with a primary peak centered around 8 nm, indicating the dominance of gel pores. In cement mortars, however, the primary peak was around 40 nm, suggesting that capillary pores were predominant [71].

Variations in the distribution of gel pores in geopolymer mortars may serve as an indicator of the reaction degree [79]. Geopolymers containing barite powder exhibited the highest content of gel pores, which could imply a slightly lower reaction degree compared to the reference mortar. However, upon examining the SEM microphotographs, it appears that a high porosity observed in geopolymers is largely due to microcracks and large voids left by fly ash cenospheres, which are not detectable via BET analysis. This explains the lower flexural and compressive strengths of fly ash geopolymer mortars. Nonetheless, the increasing presence of gel pores resulting from the addition of barite does not appear to negatively impact the mechanical properties of geopolymer mortar.

Table 8
The BET surface area and BJH pore volume of geopolymer and cement based mortars modified by barite powder.

Specimen	Surface area ($m^2\ g^{-1}$)	Pore volume ($cm^3\ g^{-1}$)	Gel pores (<10 nm) (%)	Other mesopores and macropores (%)
GEO	4.99	0.067	63.48	36.52
GEO-B-10	6.53	0.085	58.86	41.14
GEO-B-20	8.59	0.102	60.16	39.84
CEM	6.77	0.097	52.72	47.28
CEM-B-10	8.03	0.104	46.91	53.09
CEM-B-20	7.68	0.102	44.22	55.78

3.4. Gamma-ray attenuation parameters

The gamma-ray attenuation parameters for the five-layer specimens, including the linear attenuation coefficient (μ), tenth-value layer (TVL), and the half-value layer (HVL), are presented in Table 9. The results indicate that the cement reference mortar, containing 100 % normal-density sand, has a higher linear attenuation coefficient and lower TVL and HVL compared to the geopolymer reference mortar with the same type of sand. For both geopolymer and cement-based mortars, the influence of barite is noticeable. As the barite content increases, there is a clear rise in μ and a corresponding decrease in HVL and TVL. This effect is slightly more pronounced in the cement mortars. The increase in the linear absorption coefficient from the reference CEM to the CEM-B-20 cement mortars was 10 %, while the corresponding increase between GEO and GEO-B-20 geopolymer mortars was 7 %. Similarly, the decrease in the tenth-value layer was 9 % for cement mortars and 6 % for geopolymer mortars.

The mass attenuation coefficient, which normalized the attenuation coefficient by the material's density, exhibits the opposite trend. While the values for cement-based mortars remained relatively unchanged as barite content increased, they decreased by 6 % between the GEO and GEO-B-20 geopolymer mixtures. Nonetheless, the mass attenuation coefficient of the geopolymer was higher than of reference cement mortar, implying that geopolymer exhibits better shielding properties for materials of the same density compared to cement-based mortars.

The results of gamma radiation attenuation from a ^{137}Cs source clearly demonstrate differences between geopolymer and cement-based mortars, as well as the influence of barite filler. Gopolymer mortars exhibited a lower linear attenuation coefficient and higher TVL and HVL compared to cement-based mortars, yet a higher mass attenuation

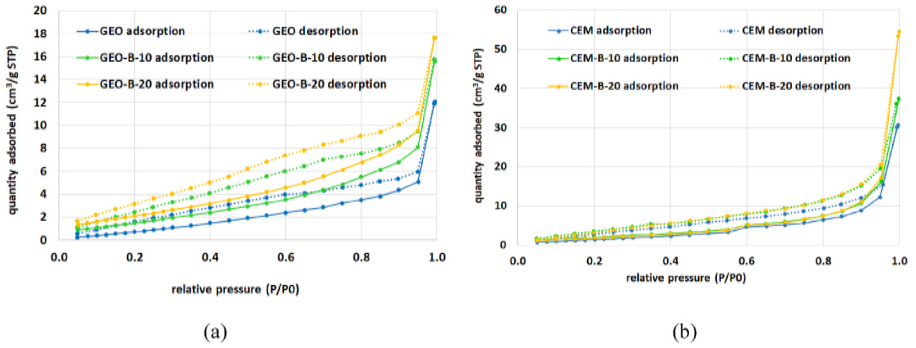

Fig. 8. Nitrogen adsorption and desorption isotherm characteristics of hardened: (a) fly ash geopolymer and (b) cement mortar.

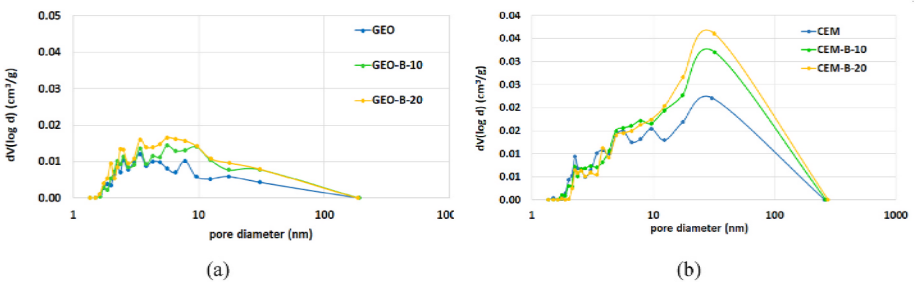

Fig. 9. BJH results of hardened: (a) fly ash geopolymer and (b) cement mortar; pore characteristics – dV(logd).

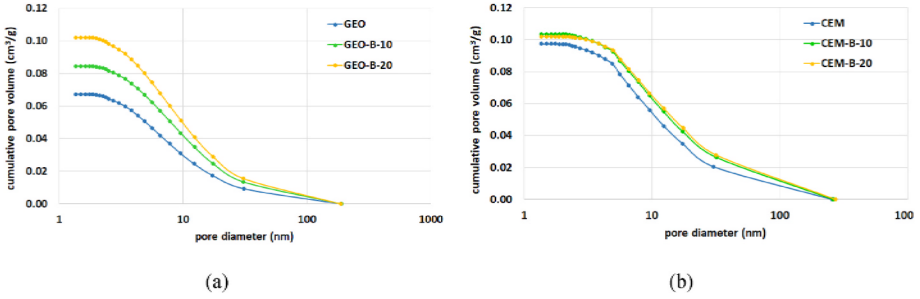

Fig. 10. BJH results of hardened: (a) fly ash geopolymer and (b) cement mortar; pore characteristics – cumulative pore volume.

Table 9
The results of the attenuation of ^{137}Cs gamma radiation for analyzed specimens.

Specimen description	Linear attenuation coefficient	Uncertainty of μ	Mass attenuation coefficient	Half-value layer	Tenth-value layer
	μ (cm^{-1})	u_μ (cm^{-1})	μ_m ($cm^2\ g^{-1}$)	HVL (cm)	TVL (cm)
CEM	0.1746	0.0008	0.0783	3.97	13.19
CEM-B-10	0.1840	0.0005	0.0793	3.77	12.51
CEM-B-20	0.1920	0.0013	0.0787	3.61	11.99
GEO	0.1695	0.0003	0.0839	4.09	13.58
GEO-B-10	0.1752	0.0013	0.0811	3.96	13.14
GEO-B-20	0.1812	0.0015	0.0789	3.83	12.71

coefficient. Hassan et al. [52] analyzed concrete and geopolymer made with blast furnace slag or fly ash and found that slag-based geopolymer achieved the highest linear and mass attenuation coefficient (0.1642 cm^{-1}; 0.782 $cm^2\ g^{-1}$, respectively) compared to fly ash-based geopolymer (0.1387 cm^{-1}; 0.761 $cm^2\ g^{-1}$) and ordinary concrete (0.1380 cm^{-1}; 0.730 $cm^2\ g^{-1}$) when subjected to ^{137}Cs gamma irradiation. Similarly, Catenacci et al. [55] reported that the linear attenuation coefficient of mortars exposed to ^{60}Co gamma irradiation decreased in the following order: slag-based geopolymer, fly ash-based geopolymer, and cement-based mortar. In the conducted research, higher values for both the linear and mass attenuation coefficients were obtained for the reference cement mortar (0.1746 cm^{-1}; 0.783 $cm^2\ g^{-1}$) and the reference fly ash geopolymer (0.1695 cm^{-1}; 0.839 $cm^2\ g^{-1}$).

The relationship between μ and density in the analyzed mortars is shown in Fig. 11, alongside literature data for cement and fly ash geopolymer mortars [55], fly ash geopolymer and cementitious concretes containing barite [80], and ordinary concretes [81]. Fig. 11 illustrates that for both geopolymer-based and cement-based mortars, there is a direct relationship between density and μ. Specifically, as the density of the mortar increases, the linear absorption coefficient also increases. This is consistent with theoretical expectations because denser materials contain more mass per unit volume, which enhances their ability to absorb radiation. The data aligns well the trend reported by NIST for the ordinary concrete, which reinforces the reliability of the observed relationship between density and the linear absorption coefficient in the tested materials.

Fig. 12 illustrates the relationship between the half-value layer and the density of geopolymer and cement-based mortars. This figure is key for understanding how effective these materials are at attenuating radiation, particularly in terms of the HVL, which is a crucial parameter

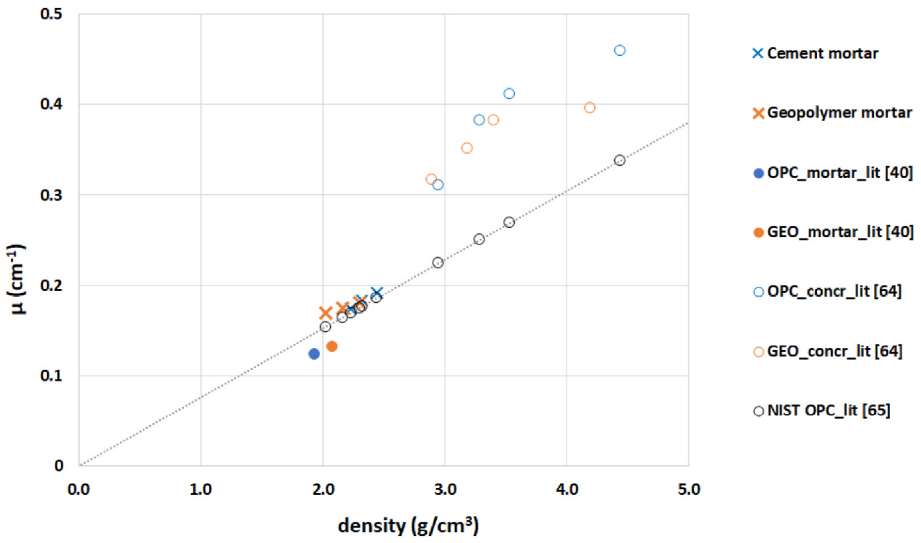

Fig. 11. The relationship between linear absorption coefficient μ and density of the geopolymer and cement based mortars compared to literature data; OPC – ordinary Portland concrete.

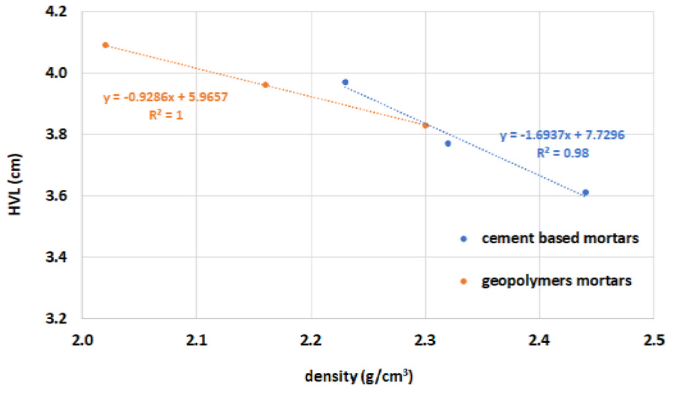

Fig. 12. The relationship between the half-value layer and density of the geopolymer and cement based mortars.

for radiation shielding applications. As shown in Fig. 12, there is a clear relationship between HVL and density for both geopolymer and cement-based mortars. This relationship aligns with the general principle that denser materials tend to have lower HVL values because they provide more mass for radiation to interact with, resulting in more effective attenuation. As known, with increasing concrete denisty, HVL and TVL values decrease [72]. The results in Fig. 12 demonstrate that the HVL of both geopolymer and cement-based composites is comparable, falling within a range of 3.6–4.1 cm. This indicates that both types of materials – geopolymers and traditional cement-based mortars – perform similarly when it comes to radiation shielding. However, the critical point is that fly ash-based geopolymers achieve these HVL values with lower material densities compared to traditional cement-based mortars. This suggests that geopolymer mortars, particularly those made with fly ash, are more efficient in terms of radiation attenuation relative to their density. In other words, less material mass is required to achieve the same level of radiation shielding as cement-based mortars.

4. Conclusions

The present study reports a comprehensive dataset on the mineralogical (XRD), structural (FTIR), microstructural (SEM), and mechanical properties of cement-based and fly ash geopolymer mortars with varying amounts of barite powder as a partial replacement for quartz sand. All mixtures were exposed to gamma irradiation from a ^{137}Cs source.

Cement mortars exhibited 23–25 % higher compressive and flexural strengths compared to fly ash geopolymer mortars. This difference is likely due to the well-established hydration reactions in cement, which form stronger C-S-H gel, a known contributor to mechanical strength. However, both mortar types saw an improvement in mechanical properties when part of the sand was replaced with barite powder, indicating that barite's high density positively influences the structural integrity, particularly in geopolymer mortars.

The pore structure varied significantly between the two mortar types. Cement-based mortars had a 30 % higher surface area and cumulative pore volume compared to geopolymer mortars, with capillary pores dominating the structure. In contrast, the fly ash geopolymer mortars had a greater proportion of gel pores, which contributed to their lower overall porosity. The addition of barite powder had little effect on the cement mortars but significantly increased the volume of gel pores in the geopolymer mortars. These findings align with the scientific understanding that geopolymer gels tend to form fewer, smaller pores compared to the capillary pore structure typical of cementitious binders.

Microstructural analysis revealed that the addition of barite powder had minimal impact on the chemical reaction products in both types of binders, but it slightly enhanced pore refinement in geopolymers. Despite this, geopolymers were more prone to crack formation, particularly under flexural stress, which reduced their flexural strength. This behavior can be explained by the brittleness of geopolymer networks compared to cementitious matrices, which are more resilient under tensile or bending loads.

Cement mortars with 100 % normal-density sand had a higher linear attenuation coefficient (μ) and correspondingly lower HVL and TVL values compared to geopolymer mortars. This suggests that the higher density of cement-based materials provides better shielding efficiency against gamma rays. However, geopolymers exhibited a higher mass attenuation coefficient, meaning they could achieve comparable gamma-ray attenuation at lower densities, which underscores their potential as lightweight radiation shielding materials. This observation is supported by the scientific theory that geopolymer materials, with their unique chemical composition, can offer effective attenuation despite their lower density compared to cement.

Regardless of the mortar composition, adding barite powder improved the gamma-ray shielding properties by 7–10 %. This enhancement can be attributed to barite's high atomic number and density, which increase the material's overall ability to absorb radiation. Barite acts as an effective filler for increasing the density of the material,

thus reducing both the HVL and TVL values, which is consistent with theoretical expectations in radiation physics.

These findings demonstrate that while traditional cement mortars offer higher mechanical strength, fly ash geopolymers, particularly when modified with barite powder, present a viable alternative for applications requiring sustainable materials with efficient radiation shielding capabilities. This combination of properties makes geopolymer mortars especially promising for specialized construction applications, such as in radiation-sensitive environments.

Future research could explore how different special aggregates can enhance gamma and neutron shielding properties in geopolymer-based materials without compromising mechanical performance, while also ensuring long-term durability, particularly in relation to long-lived radioisotopes.

CRediT authorship contribution statement

Daria Jóźwiak-Niedźwiedzka: Writing – review & editing, Writing – original draft, Validation, Supervision, Methodology, Investigation, Formal analysis, Conceptualization. **Pavel Rovnaník:** Writing – review & editing, Writing – original draft, Validation, Resources, Investigation, Formal analysis, Conceptualization. **Mariusz Dąbrowski:** Writing – review & editing, Investigation. **Jakub Ośko:** Writing – review & editing, Writing – original draft, Investigation, Formal analysis. **Michał Kuć:** Writing – review & editing, Investigation. **Maciej Maciak:** Writing – review & editing, Investigation.

Data availability

Original data are available on the request.

Declaration of competing interest

The authors declare that they have no known competing financial interests or personal relationships that could have appeared to influence the work reported in this paper.

Acknowledgement

The financial support of Brno University of Technology under the FAST-S-23-8318 project is gratefully acknowledged.

References

[1] M.-S. Kim, S.-C. Han, J.-I. Yun, Effect of supplementary cementitious materials on the degradation of cement-based barriers in radioactive waste repository: a case study in Korea, Nucl. Eng. Technol. 56 (2024) 123–130, https://doi.org/10.1016/j.net.2024.04.041.

[2] D.S. Wisnubroto, H. Zamroni, R. Sumarbagiono, G. Nurliati, Challenges of implementing the policy and strategy for management of radioactive waste and nuclear spent fuel in Indonesia, Nucl. Eng. Technol. 53 (2) (2021) 549–561, https://doi.org/10.1016/j.net.2020.07.005.

[3] The Behaviours of Cementitious Materials in Long Term Storage and Disposal: an Overview of Results of the IAEA Coordinated Research Project. IAEA-TECDOC, 1701, International Atomic Energy Agency, 2013.

[4] Z. Drace, M.I. Ojovan, Cementitious materials for radioactive waste management within IAEA Coordinated Research Project, in: Proceedings of the International Conference on Radioactive Waste Management and Environmental Remediation, ICEM, 2011, pp. 5–13, https://doi.org/10.1115/ICEM2011-59021.

[5] F. Akman, H. Ogul, I. Ozkan, M.R. Kaçal, O. Agar, H. Polat, K. Dilsiz, Study on gamma radiation attenuation and non-ionizing shielding effectiveness of niobium-reinforced novel polymer composite, Nucl. Eng. Technol. 54 (1) (2022) 283–292, https://doi.org/10.1016/j.net.2021.07.006.

[6] S. Barbhuiya, B.B. Das, T. Qureshi, D. Adak, Cement-based solidification of nuclear waste: mechanisms, formulations and regulatory considerations, J. Environ. Manag. 356 (2024) 120712, https://doi.org/10.1016/j.jenvman.2024.120712.

[7] N.J. Abualroos, K.A. Yaacob, R. Zainon, Radiation attenuation effectiveness of polymer-based radiation shielding materials for gamma radiation, Radiat. Phys. Chem. 212 (2023) 111070, https://doi.org/10.1016/j.radphyschem.2023.111070.

[8] K. Mokhtari, M. Kheradmand Saadi, H. Ahmadpanahi, Gh Jahanfarnia, Fabrication, characterization, simulation and experimental studies of the ordinary concrete reinforced with micro and nano lead oxide particles against gamma radiation, Nucl. Eng. Technol. 53 (2021) 3051–3057, https://doi.org/10.1016/j.net.2021.04.001.

[9] B.K. Soni, R. Makwana, S. Mukherjee, N.L. Singh, K. Katovsky, Different concrete compositions as a reactor shielding material for neutrons and gamma rays, Proceedings of the DAE Symp. on Nucl. Phys. 63 (2018) 1080–1081.

[10] I. Akkurt, C. Basyigit, S. Kilincarslan, B. Mavi, A. Akkurt, Radiation shielding of concretes containing different aggregates, Cem. Concr. Compos. 28 (2) (2006) 153–157, https://doi.org/10.1016/j.cemconcomp.2005.09.006.

[11] William, K., Xi, Y., Naus, D. A Review of the Effects of Radiation on Microstructure and Properties of Concretes Used in Nuclear Power Plants, NUREG/CR-7171, ORNL/TM-2013/263, Division of Engineering Office of Nuclear Regulatory Research, U.S. Nuclear Regulatory Commission, Washington, DC 20555-0001, pp. 131.

[12] F. Becker, D. Köhnke, M. Reichardt, H. Budelmann, Investigation of various concrete compositions with respect to gamma-radiation transmission properties of Cs-137, Radiat. Phys. Chem. 171 (2020) 108679, https://doi.org/10.1016/j.radphyschem.2020.108679.

[13] S.H. Al-Tersawy, R.A. El-Sadany, H.E.M. Sallam, Long-term behavior of normal weight concrete containing hybrid nanoparticles subjected to gamma radiation, Arch. Civ. Mech. Eng. 21 (9) (2021) 1–18, https://doi.org/10.1007/s43452-020-00157-4.

[14] A. Mesbahi, H. Ghiasi, Shielding properties of the ordinary concrete loaded with micro- and nano-particles against neutron and gamma radiations, Appl. Radiat. Isot. 136 (2018) 27–31, https://doi.org/10.1016/j.apradiso.2018.02.004.

[15] Y. Zhou, X. Chen, Y. Zhan, F. Sun, J. Zhang, W. He, Research on the shielding performance of concrete in a 60Co irradiation environment, Nucl. Eng. Des. 413 (2023) 112575, https://doi.org/10.1016/j.nucengdes.2023.112575.

[16] M. Rashad, H.A. Saudi, H.M.H. Zakaly, S.A.M. Issa, A.M. Abd-Elnaiem, Control optical characterizations of Ta^{+5}–doped B_2O_3–Si_2O–CaO–BaO glasses by irradiation dose, Opt. Mater. 112 (2021) 110613, https://doi.org/10.1016/j.optmat.2020.110613.

[17] S.A.M. Issa, M. Rashad, T.A. Hanafy, Y.B. Saddeek, Experimental investigations on elastic and radiation shielding parameters of WO_3-B_2O_3-TeO_2 glasses, J. Non-Cryst. Solids 544 (2020) 120207, https://doi.org/10.1016/j.jnoncrysol.2020.120207.

[18] N.R. Abd Elwahab, N. Helal, T. Mohamed, F. Shahin, F.M. Ali, New shielding composite paste for mixed fields of fast neutrons and gamma rays, Mater. Chem. Phys. 233 (2019) 249–253, https://doi.org/10.1016/j.matchemphys.2019.05.059.

[19] S.S. Amritphale, A. Anshul, N. Chandra, N. Ramakrishnan, A novel process for making radiopaque materials using bauxite—red mud, J. Eur. Ceram. Soc. 27 (4) (2007) 1945–1951, https://doi.org/10.1016/j.jeurceramsoc.2006.05.106.

[20] G. Tyagi, A. Singhal, S. Routroy, D. Bhunia, M. Lahoti, Radiation shielding concrete with alternate constituents: an approach to address multiple hazards, J. Hazard Mater. 404 (Part B) (2021) 124201, https://doi.org/10.1016/j.jhazmat.2020.124201.

[21] S.S. Hossain, P.K. Roy, C.J. Bae, Utilization of waste rice husk ash for sustainable geopolymer: a review, Construct. Build. Mater. 310 (2021) 125218, https://doi.org/10.1016/j.conbuildmat.2021.125218.

[22] J. He, Y. Jie, J. Zhang, Y. Yu, G. Zhang, Synthesis and characterization of red mud and rice husk ash-based geopolymer composites, Cem. Concr. Compos. 37 (2013) 108–118, https://doi.org/10.1016/j.cemconcomp.2012.11.010.

[23] F. Matalkah, P. Soroushian, A. Balchandra, A. Peyvandi, Characterization of alkali-activated nonwood biomass ash–based geopolymer concrete, J. Mater. Civ. Eng. 29 (4) (2017) 04016270, https://doi.org/10.1061/(ASCE)MT.1943-5533.0001801.

[24] N. Bheel, P. Awoyera, I.A. Shar, S.A. Abbasi, S.H. Khahro, K.A. Prakash, Synergic effect of millet husk ash and wheat straw ash on the fresh and hardened properties of metakaolin-based self-compacting geopolymer concrete, Case Stud. Constr. Mater. 15 (2021) e00729, https://doi.org/10.1016/j.cscm.2021.e00729.

[25] A. Wongsa, K. Boonserm, C. Waisurasingha, V. Sata, P. Chindaprasirt, Use of municipal solid waste incinerator (MSWI) bottom ash in high calcium fly ash geopolymer matrix, J. Clean. Prod. 148 (2017) 49–59, https://doi.org/10.1016/j.jclepro.2017.01.147.

[26] S.M. Qaidi, B.A. Tayeh, H.F. Isleem, A.R. de Azevedo, H.U. Ahmed, W. Emad, Sustainable utilization of red mud waste (bauxite residue) and slag for the production of geopolymer composites: a review, Case Stud. Constr. Mater. 16 (2022) e00994, https://doi.org/10.1016/j.cscm.2022.e00994.

[27] S. Singh, M.U. Aswath, R.V. Ranganath, Performance assessment of bricks and prisms: red mud based geopolymer composite, J. Build. Eng. 32 (2020) 101462, https://doi.org/10.1016/j.jobe.2020.101462.

[28] M. Sarkar, K. Dana, Partial replacement of metakaolin with red ceramic waste in geopolymer, Ceram. Int. 47 (3) (2021) 3473–3483, https://doi.org/10.1016/j.ceramint.2020.09.191.

[29] P. Rovnaník, P. Rovnaníková, M. Vysvaril, S. Grzeszczyk, E. Janowska-Renkas, Rheological properties and microstructure of binary waste red brick powder/metakaolin geopolymer, Construct. Build. Mater. 188 (2018) 924–933, https://doi.org/10.1016/j.conbuildmat.2018.08.150.

[30] P. Duxson, A. Fernández-Jiménez, J.L. Provis, G.C. Lukey, A. Palomo, J.S.J. van Deventer, Geopolymer technology: the current state of the art, J. Mater. Sci. 42 (9) (2007) 2917–2933, https://doi.org/10.1007/s10853-006-0637-z.

[31] A. Fernández-Jiménez, A. Palomo, J.Y. Pastor, A. Martín, New cementitious materials based on alkali-activated fly ash: performance at high temperatures, J. Am. Ceram. Soc. 91 (10) (2008) 3308–3314, https://doi.org/10.1111/j.1551-2916.2008.02625.x.

[32] G. Kovalchuk, A. Fernández-Jiménez, A. Palomo, Alkali-activated fly ash: relationship between mechanical strength gains and initial ash chemistry, Mater. Constr. 58 (291) (2008) 35–52, https://doi.org/10.3989/mc.2008.v58.i291.101.

[33] C.A. Rees, J.L. Provis, G.C. Lukey, J.S.J. van Deventer, In situ ATR-FTIR study of the early stages of fly ash geopolymer gel formation, Langmuir 23 (17) (2007) 9076–9082, https://doi.org/10.1021/la701185g.
[34] S. Fernando, C. Gunasekara, D.W. Law, et al., Investigation of the reaction mechanism of blended fly ash and rice husk ash alkali-activated binders, Arch. Civ. Mech. Eng. 22 (24) (2022) 1–15, https://doi.org/10.1007/s43452-021-00349-6.
[35] F. Skvára, L. Kopecky, J. Nemecek, Z. Bittnar, Microstructure of geopolymer materials based on fly ash, Ceram. Silikaty 50 (4) (2006) 208–215. https://www.ceramics-silikaty.cz/2006/pdf/2006_04_208.pdf.
[36] J. Temuujin, R.P. Williams, A. van Riessen, Effect of mechanical activation of fly ash on the properties of geopolymer cured at ambient temperature, J. Mater. Process. Technol. 209 (12–13) (2009) 5276–5280, https://doi.org/10.1016/j.jmatprotec.2009.03.016.
[37] A. Mehta, R. Siddique, Sulfuric acid resistance of fly ash based geopolymer concrete, Construct. Build. Mater. 146 (2017) 136–143, https://doi.org/10.1016/j.conbuildmat.2017.04.077.
[38] T.A. Aiken, J. Kwasny, W. Sha, Resistance of fly ash geopolymer binders to organic acids, Mater. Struct. 53 (5) (2020) 115, https://doi.org/10.1617/s11527-020-01549-x.
[39] A. Fernández-Jiménez, I. García-Lodeiro, A. Palomo, Durability of alkali-activated fly ash cementitious materials, J. Mater. Sci. 42 (9) (2007) 3055–3065, https://doi.org/10.1007/s10853-006-0584-8.
[40] I. García-Lodeiro, A. Palomo, A. Fernández-Jiménez, Alkali-aggregate reaction in activated fly ash systems, Cem. Concr. Res. 37 (2) (2007) 175–183, https://doi.org/10.1016/j.cemconres.2006.11.002.
[41] P. Rovnaník, Fly ash geopolymer after exposure to elevated temperature: mechanical properties and microstructure, in: V. Bílek, Z. Keršner (Eds.), Non-Traditional Cement & Concrete IV, Brno University of Technology, Brno, 2011, pp. 130–138.
[42] O. Rivera, W. Long, C. Weiss Jr, R. Moser, B. Williams, K. Torres-Cancel, E. Gore, P. Allison, Effect of elevated temperature on alkali-activated geopolymeric binders compared to portland cement-based binders, Cem. Concr. Res. 90 (2016) 43–51, https://doi.org/10.1016/j.cemconres.2016.09.013.
[43] P. Rovnaník, K. Šafránková, Thermal behaviour of metakaolin/fly ash geopolymers with chamotte aggregate, Materials 9 (7) (2016) 535, https://doi.org/10.3390/ma9070535.
[44] B. Mast, I. Gerardy, Y. Pontikes, W. Schroeyers, B. Reniers, P. Samyn, G. Gryglewicz, B. Vandoren, S. Schreurs, The effect of gamma radiation on the mechanical and microstructural properties of Fe-rich inorganic polymers, J. Nucl. Mater. 521 (2019) 126–136, https://doi.org/10.1016/j.jnucmat.2019.04.045.
[45] M. Ramadan, W. Ramadan, F. Shwita, N. El-Faramawy, Valorization of hazardous glass wastes via geopolymer production utilized in gamma ray shielding applications: a comparative study with Portland cement, Radiat. Phys. Chem. 197 (2022) 110174, https://doi.org/10.1016/j.radphyschem.2022.110174.
[46] H.M. Khater, W. Ramadan, M. Gharieb, Impact of alkali activated mortar incorporating different heavy metals on immobilization proficiency using gamma rays attenuation, Prog. Nucl. Energy 137 (2021) 103729, https://doi.org/10.1016/j.pnucene.2021.103729.
[47] S. Singh, A. Kumar, D. Singh, K.S. Thind, G.S. Mudahar, Barium–borate–flyash glasses: as radiation shielding materials, Nucl. Instrum. Methods Phys. Res. B 266 (1) (2008) 140–146, https://doi.org/10.1016/j.nimb.2007.10.018.
[48] S. Shalbi, M. Jaafar, N. Ahmed, A. Al-Jarrah, A. Naji, M. Qaeed, Equivalent thicknesses of lead and fly ash geopolymer with addition of barium sulphate in radiation protection, J. Appl. Phys. 9 (1 Ver. II) (2017) 51–56, https://doi.org/10.9790/4861-0901025156.
[49] E. Phillip, T.F. Choo, N.W.A. Khairuddin, R.O. Abdel Rahman, On the sustainable utilization of geopolymers for safe management of radioactive waste: a review, Sustainability 15 (2) (2023) 1117, https://doi.org/10.3390/su15021117.
[50] L. Rubinjoni, S. Stankovic, B. Loncar, The effect of 60Co gamma irradiation on coal fly-ash geopolymer paste setting time, Nucl. Technol. Radiat. Prot. 35 (2) (2020) 150–153, https://doi.org/10.2298/ntrp2002150r.
[51] M.L.Y. Yeoh, S. Ukritnukun, A. Rawal, J. Davies, B.J. Kang, K. Burrough, Z. Aly, P. Dayal, E.R. Vance, D.J. Gregg, P. Koshy, C.C. Sorrell, Mechanistic impacts of long-term gamma irradiation on physicochemical, structural, and mechanical stabilities of radiation-responsive geopolymer pastes, J. Hazard Mater. 407 (2021) 124805, https://doi.org/10.1016/j.jhazmat.2020.124805.
[52] M.W. Hasan, S. Sugiharto, S. Astutiningsih, Gamma radiation shielding properties of slag and fly ash-based geopolymers, At. Indones. 47 (3) (2021) 173–180, https://doi.org/10.17146/aij.2021.1076.
[53] S. Kök, M.S. Türetken, N. Öksüzer, H.S. Gökçe, Effect of elevated temperature on radiation shielding properties of cement and geopolymer mortars including barite aggregate and colemanite powder, Materialia 27 (2023) 101693, https://doi.org/10.1016/j.mtla.2023.101693.
[54] J. Ahn, W.-S. Kim, W. Um, Development of metakaolin-based geopolymer for solidification of sulfate-rich HyBRID sludge waste, J. Nucl. Mater. 518 (2019) 247–255, https://doi.org/10.1016/j.jnucmat.2019.03.008.
[55] M.J. Catenacci, H.R. Luckarift, R.J. Friedman, A. Male, J.R. Owens, Effect of fly ash composition and component quantities on the gamma radiation shielding properties of geopolymer, Prog. Nucl. Energy 140 (2021) 103889, https://doi.org/10.1016/j.pnucene.2021.103889.
[56] L. Leay, A. Potts, T. Donoclift, Geopolymers from fly ash and their gamma irradiation, Mater. Lett. 227 (2018) 240–242, https://doi.org/10.1016/j.matlet.2018.05.088.
[57] European Standard EN 196-1:2016-07. Methods of Testing Cement. Determination of Strength.
[58] I. Ismail, S.A. Bernal, J.L. Provis, S. Hamdan, J.S.J. van Deventer, Drying-induced changes in the structure of alkali-activated pastes, J. Mater. Sci. 48 (9) (2013) 3566–3577, https://doi.org/10.1007/s10853-013-7152-9.
[59] G. Liang, W. Yao, A. She, New insights into the early-age reaction kinetics of metakaolin geopolymer by 1H low-field NMR and isothermal calorimetry, Cem. Concr. Compos. 137 (2023) 104932, https://doi.org/10.1016/j.cemconcomp.2023.104932.
[60] European Standard EN 61331-1:2014. Protective Devices against Diagnostic Medical X-Radiation - Part 1: Determination of Attenuation Properties of Materials.
[61] S. Domanski, M.A. Gryzinski, M. Maciak, L. Murawski, P. Tulik, K. Tyminska, Experimental investigation on radiation shielding of high performance concrete for nuclear and radiotherapy facilities, Polish J. Med. Phys. Eng. 22 (2) (2016) 41–47, https://doi.org/10.1515/pjmpe-2016-0008.
[62] M. Zielczyński, N. Golnik, Recombination Ionization Chambers, vol. 3, Monografie IEA, 2000. IAE, Otwock Świerk.
[63] K. Rajczyk, G. Janus, Microstructure and properties of geopolymers formed in the alkali activation process of fly ash, Cement-Wapno-Beton 26 (4) (2021) 279–293, https://doi.org/10.32047/cwb.2021.26.4.2.
[64] T.M. Ansari, I.L. Marr, A.M. Coats, Characterisation of mineralogical forms of barium and trace heavy metal impurities in commercial barytes by EPMA, XRD and ICP-MS, J. Environ. Monit. 3 (1) (2001) 133–138, https://doi.org/10.1039/B007943J.
[65] M. Dąbrowski, M.A. Glinicki, K. Dziedzic, D. Jóźwiak-Niedźwiedzka, S. Sikorin, V. S. Fateev, E.I. Povalansky, Early age hardening of concrete with heavy aggregate in gamma radiation source – impact on the modulus of elasticity and microstructural features, J. Adv. Concr. Technol. 19 (5) (2021) 555–570, https://doi.org/10.3151/jact.19.555.
[66] M. Horgnies, J. Chen, C. Bouillon, Overview about the use of Fourier transform infrared spectroscopy to study cementitious materials, in: 6th International Conference on Computational Methods and Experimental Measurements for Surface Effects and Contact Mechanics, WIT Transactions on Engineering Sciences, vol. 77, 2013, pp. 251–262, https://doi.org/10.2495/MC130221.
[67] B.J. Saikia, Spectroscopic estimation of geometrical structure elucidation in natural SiO_2 crystal, J. Mater. Phys. Chem. 2 (2) (2014) 28–33, https://doi.org/10.12691/jmpc-2-2-3.
[68] P. Rożek, M. Król, W. Mozgawa, Spectroscopic studies of fly ash-based geopolymers, Spectrochim. Acta Mol. Biomol. Spectrosc. 198 (2018) 283–289, https://doi.org/10.1016/j.saa.2018.03.034.
[69] H.H. Adler, P.F. Kerr, Variations in infrared spectra molecular symmetry and site symmetry of sulfate minerals, Am. Mineral. 50 (1–2) (1965) 132–147. http://www.minsocam.org/ammin/AM50/AM50_132.pdf.
[70] Y. Shen, C. Li, X. Zhu, Study on the preparation and formation mechanism of barium sulphate nanoparticles modified by different organic acids, J. Chem. Sci. 119 (4) (2007) 319–324, https://doi.org/10.1007/s12039-007-0043-3.
[71] M. Lahoti, S.F. Wijaya, K.H. Tan, E.H. Yang, Tailoring sodium-based fly ash geopolymers with variegated thermal performance, Cem. Concr. Compos. 107 (2020) 103507, https://doi.org/10.1016/j.cemconcomp.2019.103507.
[72] A. Fernández-Jiménez, M. Monzó, M. Vicent, A. Barba, A. Palomo, Alkaline activation of metakaolin-fly ash mixtures: obtain of zeoceramics and zeocements, Microporous Mesoporous Mater. 108 (1–3) (2008) 41–49, https://doi.org/10.1016/j.micromeso.2007.03.024.
[73] T. Shi, Y. Gao, D.J. Corr, FTIR study on early-age hydration of carbon nanotubes-modified cement-based materials, Adv. Cement Res. 31 (8) (2019) 353–361, https://doi.org/10.1680/jadcr.16.00167.
[74] J. Kalkreuth, A. Ullrich, K. Garbev, Accelerated carbonation of hardened cement paste: quantification of calcium carbonate via ATR infrared spectroscopy, J. Am. Ceram. Soc. (2022), https://doi.org/10.1111/jace.19546.
[75] K. Saidani, L. Ajam, M. Ben Ouezdou, Barite powder as sand substitution in concrete: effect on some mechanical properties, Construct. Build. Mater. 95 (2015) 287–295, https://doi.org/10.1016/j.conbuildmat.2015.07.150.
[76] R. Tomczak, M. Wyrzykowski, J.A. Stegemann, Performance of fly ash based geopolymer concrete beams subjected to flexure and shear, Case Stud. Constr. Mater. 16 (2022) e00896, https://doi.org/10.1016/j.cscm.2022.e00896.
[77] H.S. Gökçe, Ç. Yalçınkaya, M. Tuyan, Optimization of reactive powder concrete by means of barite aggregate for both neutrons and gamma rays, Construct. Build. Mater. 189 (2018) 470–477, https://doi.org/10.1016/j.conbuildmat.2018.09.022.
[78] M. Heikal, T. Bayoumi, M. Sami, S. Abo-El-Enein, Effect of gamma irradiation on fresh properties of metakaolin-based geopolymer paste, in: 9th International Conference on Borate Glasses, Crystals and Melts & 2nd International Conference on Phosphate Materials, Montpellier, France, 2016.
[79] W. Kurniawan, N.H. Apriantoro, The effects of gamma irradiation on the microstructure and mechanical properties of fly ash-based geopolymer mortar, Materials 12 (19) (2019) 3197, https://doi.org/10.3390/ma12193197.
[80] M. Reichardt, F. Becker, H. Budelmann, D. Köhnke, Influence of gamma radiation on the physical and mechanical properties of cementitious materials with different compositions, Nucl. Eng. Des. 336 (2018) 148–160, https://doi.org/10.1016/j.nucengdes.2018.07.026.
[81] X-ray mass attenuation coefficients [Online]. Available: https://physics.nist.gov/PhysRefData/XrayMassCoef/ComTab/concrete.html. (Accessed 4 December 2023).